ADVANCED ENERGY MATERIALS

www.advenergymat.de

Slurry-Fabricable Li$^+$-Conductive Polymeric Binders for Practical All-Solid-State Lithium-Ion Batteries Enabled by Solvate Ionic Liquids

*Dae Yang Oh, Young Jin Nam, Kern Ho Park, Sung Hoo Jung, Kyu Tae Kim, A. Reum Ha, and Yoon Seok Jung**

For mass production of all-solid-state lithium-ion batteries (ASLBs) employing highly Li$^+$ conductive and mechanically sinterable sulfide solid electrolytes (SEs), the wet-slurry process is imperative. Unfortunately, the poor chemical stability of sulfide SEs severely restrict available candidates for solvents and in turn polymeric binders. Moreover, the binders interrupt Li$^+$-ionic contacts at interfaces, resulting in the below par electrochemical performance. In this work, a new scalable slurry fabrication protocol for sheet-type ASLB electrodes made of Li$^+$-conductive polymeric binders is reported. The use of intermediate-polarity solvent (e.g., dibromomethane) for the slurry allows for accommodating Li_6PS_5Cl and solvate-ionic-liquid-based polymeric binders (NBR-Li(G3)TFSI, NBR: nitrile–butadiene rubber, G3: triethylene glycol dimethyl ether, LiTFSI: lithium bis(trifluoromethanesulfonyl)imide) together without suffering from undesirable side reactions or phase separation. The $LiNi_{0.6}Co_{0.2}Mn_{0.2}O_2$ and $Li_4Ti_5O_{12}$ electrodes employing NBR-Li(G3)TFSI show high capacities of 174 and 160 mA h g^{-1} at 30 °C, respectively, which are far superior to those using conventional NBR (144 and 76 mA h g^{-1}). Moreover, high areal capacity of 7.4 mA h cm^{-2} is highlighted for the $LiNi_{0.7}Co_{0.15}Mn_{0.15}O_2$ electrodes with ultrahigh mass loading of 45 mg cm^{-2}. The facilitated Li$^+$-ionic contacts at interfaces paved by NBR-Li(G3)TFSI are evidenced by the complementary analysis from electrochemical and ^{7}Li nuclear magnetic resonance measurements.

The electrification of powertrain and the stabilization of renewable energy sources are a major driving force to develop advanced lithium-ion batteries (LIBs) having high energy density and safety.[1–4] In this regard, all-solid-state Li metal batteries which exclude flammable organic liquid electrolytes are considered as one of the most promising solutions.[5–12] Despite the poor chemical stability (e.g., instability in atmospheric air and conventional polar solvents), sulfide solid electrolyte (SE) materials are highly promising to realize all-solid-state Li-ion or Li batteries (ASLBs) which may outperform conventional LIBs.[5,13–21] Li$^+$ conductivities of several state-of-the-art sulfide Li$^+$ superionic conductors have reached ≈10^{-2} S cm^{-1} at room temperature ($Li_{9.54}Si_{1.74}P_{1.44}S_{11.7}Cl_{0.3}$[13]: 2.5×10^{-2} S cm^{-1}, $Li_7P_3S_{11}$[22]: 1.7×10^{-2} S cm^{-1}), which is comparable to that of organic liquid electrolytes.[23] Moreover, sulfide SE materials show considerably low Young's modulus of ≈20 GPa, allowing to be sintered mechanically at room temperature.[5,15,24–27] In sharp contrast, brittle oxide SE materials showing higher Young's modulus (e.g., $Li_7La_3Zr_2O_{12}$: 150 GPa) suffer from unwanted chemical reaction with active materials during hot-sintering procedure to fabricate ASLBs.[5,24]

In the viewpoints of mass production of ASLBs using sulfide SEs, adaptation of the wet-slurry process, employed to fabricate sheet-type electrodes for conventional LIBs, is desirable.[5,16,28–31] In particular, the use of polymeric binders for sheet-type ASLB electrodes is necessary to provide with mechanical properties that are applicable to the scalable high-throughput roll-to-roll processes.[5,16,30] Moreover, the presence of "soft" polymers in the electrodes could effectively buffer chemomechanically derived stress and strain upon repeated charge and discharge cycles, and alleviate the mechanical failures such as the formation of cracks and the detachment of particles.[5,27]

Unfortunately, the development of wet slurry process for fabricating ASLB electrodes employing polymeric binders is highly challenging due to several issues. First, polymeric binders should be dissolved into nonpolar or less polar solvents such as xylene that have negligible reactivity with sulfide SEs.[16,29] Second, polymeric binders that have insufficient binding ability are excluded. It is notable that, while the dissolution of polymers into nonpolar or less polar solvents becomes favored for

D. Y. Oh, Dr. Y. J. Nam, Dr. K. H. Park, S. H. Jung, K. T. Kim, A. R. Ha, Prof. Y. S. Jung
Department of Energy Engineering
Hanyang University
Seoul 04763, South Korea
E-mail: yoonsjung@hanyang.ac.kr
D. Y. Oh, Dr. Y. J. Nam, S. H. Jung
School of Energy and Chemical Engineering
UNIST
Ulsan 44919, South Korea

The ORCID identification number(s) for the author(s) of this article can be found under https://doi.org/10.1002/aenm.201802927.

DOI: 10.1002/aenm.201802927

the ones having less polar backbones and/or branches, the binding ability (or the intermolecular force) of polymers is generally enhanced by increasing polarity.[32,33] Third, polymeric binders should be soft or flexible. Although the polymers such as polystyrene (PS) and poly(methyl methacrylate) (PMMA) are dissolved into xylene, they form poor electrodes which suffer from brittleness and peeling-off of the electrode layers, which is discussed later. The aforementioned three criteria severely restrict the availability in polymeric binders for sheet-type ASLB electrodes fabricated by wet-slurry process, e.g., nitrile–butadiene rubber (NBR) and styrene–butadiene rubber.[16,28,29,34]

Even though mechanically compliant sheet-type ASLB electrodes could be fabricated using carefully selected polymeric binders, the polymeric domains heavily interrupt the ionic contacts, resulting in the far below par electrochemical performances.[5,16,29,35] It was shown that the use of only 1.4 wt% NBR binders in the sheet-type ASLB electrodes leaded to decreases in surface coverage of SEs onto active materials approximately by half (e.g., from 25.2% to 17.5%), resulting in the significant degradation of electrochemical performances.[29] This problem calls for a research direction to develop Li^+-conductive polymeric binders that could cope with the wet-slurry process for ASLB electrodes. To this end, highly Li^+-conductive gel polymer electrolytes (≈10^{-4} S cm^{-1} at room temperature) are an appropriate candidate.[36,37] In designing Li^+-conductive gel polymer electrolyte binders for ASLBs, several aspects should be considered. First, in order not to offset the advantage ASLBs, gel polymer electrolytes having high thermal stability are desired. Second, liquid components for gel polymer electrolytes should be able to dissolve Li salts but remain intact in contact with reactive sulfide SE materials. Third, gel polymer electrolytes should be miscible with nonpolar or less polar solvents used for the slurry. These considerations led us to recent progresses in super-concentrated (or solvent-in-salt) electrolytes as the constituent for gel polymer electrolyte binders, owing to the abnormal promising properties, such as high thermal stability, extended electrochemical stability, facile charge transfer kinetics, and suppression of polysulfide dissolution.[38–42] Especially, in our previous study, we demonstrated that solvate ionic liquids (SILs), a solvent–salt complex of glyme and Li salt, such as $Li(glyme)_yX$ (X: polyanion) (e.g., Li(G3)TFSI, referred to as "LiG3," G3 is triethylene glycol dimethyl ether and LiTFSI is lithium bis(trifluoromethanesulfonyl)imide),[42,43] showed the excellent compatibility with sulfide SE materials because the strong interaction between Li^+ and electronegative elements in the polar solvents alleviates the reactivity of solvents.[44]

Based on the aforementioned research and motivations, we report on the development of flexible sheet-type ASLB electrodes tailored using slurry-fabricable Li^+-conductive polymeric binders. Solvents with intermediate polarity such as dibormomethane (DBM) are demonstrated to show inertness in contact with sulfide SEs and miscibility with SILs at the same time. Complementary analysis using electrochemical and ^7Li nuclear magnetic resonance (NMR) measurements evidences the facilitated Li^+ transport at interfaces through the NBR-SIL binders, which results in the significant improvement in electrochemical performances of $LiNi_{0.6}Co_{0.2}Mn_{0.2}O_2$ (NCM622), $LiNi_{0.7}Co_{0.15}Mn_{0.15}O_2$ (NCM711), and $Li_4Ti_5O_{12}$ (LTO) electrodes for ASLBs, compared with the sample using conventional Li^+-ion insulating binders (NBR) (NCM622 and NCM711 are also referred to as NCM more generally in the texts).

For designing ASLB slurry to accommodate SIL-based Li^+-conductive polymeric binders and sulfide SEs together, for various solvents with wide ranges of polarity (estimated by dielectric constant and dipole moment), their miscibility with LiG3 and reactivity with sulfide SE (Li_6PS_5Cl (LPSCl)) were tested (Figure S1, Table S1, Supporting Information). The mixtures of LiG3 and nonpolar solvents (e.g., toluene and *o*-xylene) showed clear separation of phases (Figure S1a, Supporting Information). In sharp contrast, the solvents with high polarity (water, acetonitrile, and N-methyl-2-pyrrolidone (NMP)) and intermediate polarity (dichloromethane, DBM, and chloroform) appeared to be miscible with LiG3. However, the highly polar solvents showed severe dissolution of sulfide SE, LPSCl, and are thus excluded for the slurry application (Figure S1b, Supporting Information). From this screening process, the solvents with intermediate polarity such as dichloromethane, DBM, and chloroform were selected as appropriate solvents for the ASLB slurry. These solvents could also dissolve NBR (Figure S2, Table S2, Supporting Information).

The comprehensive explanation on these test results is illustrated in **Figure 1**. Strong Lewis-basic (or highly polar) solvents (e.g., water, acetonitrile, and G3) having lone-pair electrons at highly electronegative elements (e.g., O and N) react with electrophilic species (e.g., P^{5+} in sulfide SEs), which is explained by hard and soft acids and bases (HSAB) theory.[44,45] Moreover, strong interaction between electronegative elements (e.g., O and N) in these solvents and Li^+ ions solvated by the G3 molecule might cleave the coordinated structure of $[Li(G3)]^+$,[43]

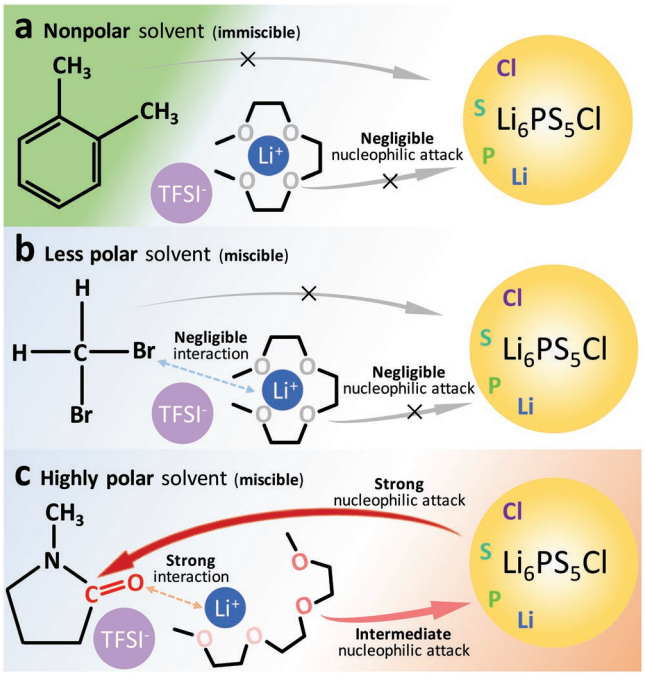

Figure 1. Schematic diagram representing reactivity with LPSCl (Li_6PS_5Cl) for LiG3 (Li(G3)TFSI) diluted by various solvents; a) nonpolar, b) less polar, and c) highly polar solvents. Note that less polar solvents with negligible donor ability are miscible with LiG3 and compatible with LPSCl (b).

leading to additional side reaction between G3 and LPSCl. For NMP, the solvent used for conventional LIB slurries, as O in carbonyl group could interact with the solvated Li^+, O in the adrift G3 could react with LPSCl (Figure 1c). Additionally, the electrophillic C in carbonyl group could be attacked by thiophosphates (e.g., PS_4^{3-} and $P_2S_7^{4-}$) in LPSCl. This rationale is in line with the chemical incompatibility between carbonate-based liquid electrolytes and polysulfides for Li–S batteries.[46] In sharp contrast, nonpolar solvents such as *o*-xylene are chemically inert in contact with LPSCl due to their negligible donor ability (Figure 1a). However, LiG3 is immiscible with nonpolar solvents because of huge difference in polarity between nonpolar solvents and G3 (Table S1, Supporting Information). Finally, the solvents having intermediate polarity with the moderately lower donor ability, especially DBM, can dilute LiG3 without disrupting the coordination structure of $[Li(G3)]^+$, and thus be chemically compatible with sulfide SEs (Figure 1b).

A composite sample of LPSCl, NBR, and LiG3, referred to as "LPSCl–NBR–LiG3" (weight ratio of 50:20:30), was prepared by dissolving NBR and diluting LiG3 into DBM, followed by dispersing LPSCl powders. After an exposure of LPSCl to DBM or compositing with NBR and LiG3 via the DBM-based slurry process, characteristic X-ray diffraction (XRD) peaks for argyrodite Li_6PS_5Cl (JCPDS no. 418490) remained unchanged without evolution of any impurities (**Figure 2**a), confirming the excellent compatibility of LPSCl with DBM and LiG3. In addition, ^7Li NMR analyses for LiG3, a composite sample of NBR and LiG3, referred to as "NBR–LiG3," and LPSCl–NBR–LiG3 were carried out to determine the local environment around Li (Figure 2b,c). Static ^7Li NMR spectra for LiG3 and NBR–LiG3 are compared in Figure 2b. The liquid-state LiG3 showed a sharp peak at –0.36 ppm, implying that Li is only shielded by O of the G3 molecule and mobile freely in a liquid phase.[47] In contrast, the broader peak was observed for NBR–LiG3. This indicates the reduced mobility of Li^+ ions, which is in line with typical observations when electrolyte is soaked into the polymeric matrix.[48] Furthermore, magic angle spinning (MAS) ^7Li NMR measurements were attempted (Figure 2c) because the broad peak of LPSCl centered at ≈2.5 ppm was overlapped with other signals from LiG3 or NBR–LiG3 at the static mode (Figure S3, Supporting Information). By comparing with the data of reference samples of LPSCl and NBR–LiG3, the distinct peaks of Li from LPSCl (2.5 ppm) and NBR–LiG3 (–0.25 ppm) were clearly observed without any other noticeable signals. This observation indicates that LiG3 does not exist to be separated from NBR, but soaked into the polymeric matrix (NBR), forming a gel polymer electrolyte. Moreover, cross-sectional field-emission scanning electron microscopy (FESEM) image of LPSCl–NBR–LiG3 films and its corresponding energy dispersive X-ray spectroscopy (EDXS) elemental maps (Figure 2d) showed the overlapped distribution of C (from NBR and LiG3), F (from LiG3), and N (from NBR and LiG3), being separated by the signals of P and S (both from LPSCl), which corroborates the formation of the NBR–LiG3 gel polymer electrolyte. Figure 2e shows the photograph of 70 μm thick LPSCl–NBR–LiG3 films, showing the excellent flexibility. Moreover, degradation of Li^+ conductivity by compositing with NBR-LiG3 was marginal; 4.2×10^{-3} S cm^{-1} for LPSCl to 3.3×10^{-3} S cm^{-1} for LPSCl–NBR–LiG3 (Table S3, Supporting Information). This result suggests that NBR–LiG3 could act as a good Li^+-conductive binder because of its high Li^+ conductivity of NBR–LiG3 (1.7×10^{-4} S cm^{-1}).

Li^+-ionic conduction pathways in LPSCl–NBR–LiG3 were investigated by MAS ^7Li NMR measurements of Li-ion nonblocking symmetric cells of ^6Li/LPSCl–NBR–LiG3/^6Li (**Figure 3**a) using ^6Li metal electrodes. The as-assembled ^6Li metal symmetric cells were cycled repeatedly at 50 μA for every 5 min to replace ^7Li in the sample (LPSCl–NBR–LiG3) with ^6Li (Figure 3b). After the cycling, the LPSCl–NBR–LiG3 sample was collected and subjected to the MAS ^7Li NMR measurements. Figure 3c displays the MAS ^7Li NMR signals of LPSCl–NBR–LiG3 before and after cycling. The intensities of both peaks for LPSCl (2.5 ppm) and NBR–LiG3 (–0.25 ppm) decreased, indicating that ^7Li in the samples were partly replaced by ^6Li from ^6Li metal electrodes. Most importantly, this observation verifies that Li^+ ions migrate through not only LPSCl but also NBR–LiG3, confirming the facilitated transport of Li^+ ions by NBR–LiG3 (or Li^+ ions move not only through the pathway 1 but also through the pathway 2, as illustrated in Figure 3a).[49,50] Furthermore, the areal ratio of ^7Li peaks for LPSCl/NBR–LiG3 decreased from 16 to 9 after cycling, indicating that more ^7Li was substituted in LPSCl than in NBR–LiG3. This result reflects that the Li^+ ion pathways are formed preferably through the LPSCl domains in the hybrid SE films, which is not surprising in that the ionic conductivity of LPSCl is higher than that of NBR–LiG3 despite a lower volumetric fraction of LPSCl (38%) in the sample.[49,50] The broadening in line at 2.5 ppm after cycling may be attributed to contribution of structurally and/or compositionally altered domains, which could originate from reduction by Li metal.[5,51–53] The control experiment by AC impedance method using Al/NBR–LiG3/LPSCl/NBR–LiG3/Al cells verifies Li^+-ion movement across the LPSCl/NBR–LiG3 interfaces (Figure S4, Supporting Information). Moreover, the interfacial resistance is obtained to be 33.8 Ω cm^2. This value is lower than those for LiG3/Li (≈150 Ω cm^2),[42] Li_3PS_4/Li (≈100 Ω cm^2),[54] and typical LIBs (62 Ω cm^2),[55] which implies facile Li^+ transport across the LPSCl/NBR–LiG3 interfaces.

The sheet-type NCM electrodes were tailored from a DBM-based slurry containing NCM, LPSCl, super C65, NBR, and LiG3, as the same procedure for preparing the LPSCl–NBR–LiG3 except for the addition of NCM and super C65 powders. The electrode composition (weight ratio) of NCM, LPSCl, super C65, NBR, and LiG3, was 70.0:(27.5 – x):1.0:1.5:*x* where *x* was varied from 0.0 to 1.0 and 3.5 (Table S4, Supporting Information). Note that high mass loading of 15 mg_{NCM622} cm^{-2} (21 $mg_{electrode}$ cm^{-2}), which is relevant to practical evaluation, was applied. The as-prepared NCM622 electrodes using the NBR–LiG3 binders (3.5 wt% LiG3) showed excellent mechanical properties; flexibility, and good adhesion of the electrode layers on Al current collectors (Figure S5b, Supporting Information). In contrast, the electrodes prepared without using NBR (or NBR–LiG3) suffer from peeling-off and breakage of the electrode layers, emphasizing the indispensible role of polymeric binders (Figure S5a, Supporting Information). Moreover, the electrode using NBR–LiG3 kept the solid-state behavior without any leakage of liquids even

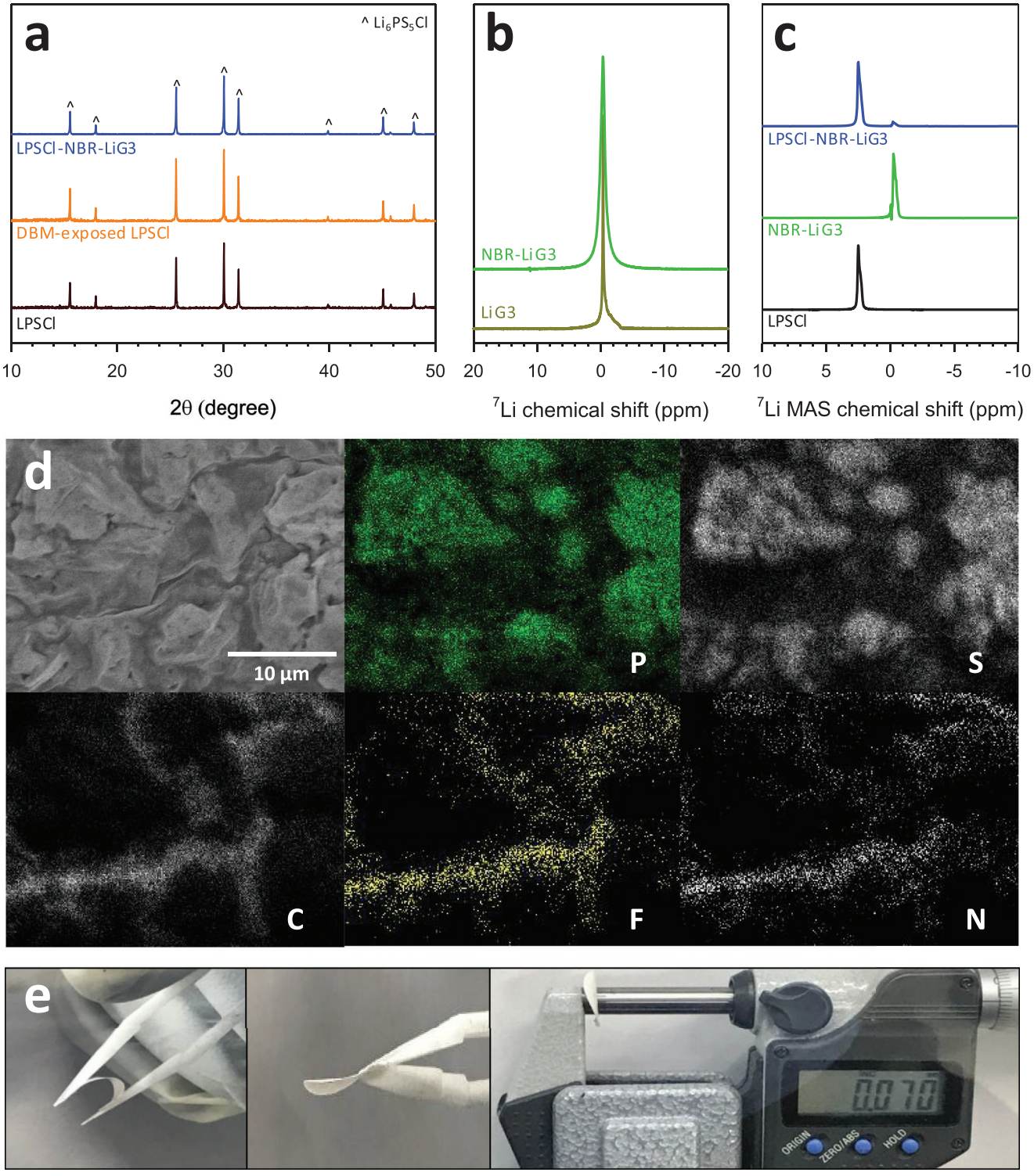

Figure 2. Characterization of LPSCl–NBR–LiG3 composites. a) XRD patterns of pristine LPSCl, DBM (dibromomethane)-exposed LPSCl, and LPSCl–NBR–LiG3. b) Static ^{7}Li NMR spectra of LiG3 and NBR–LiG3. c) MAS ^{7}Li NMR spectra of LPSCl, NBR–LiG3, and LPSCl–NBR–LiG3. d) Cross-sectional FESEM image of LPSCl–NBR–LiG3 films and its corresponding EDXS elemental maps. e) Photographs of flexible LPSCl–NBR–LiG3 films.

after pressing at 370 MPa and repeated bending (the inset in **Figure 4**a).

The advantage of facile Li^+ transports aided by Li^+-conductive binder, NBR–LiG3, was evaluated by comparing the electrochemical performances at 30 °C of all-solid-state NCM/Li–In and LTO/Li–In cells made of sheet-type electrodes using NBR–LiG3 with the ones made of NBR (Figure 4). The first-cycle charge–discharge voltage profiles of NCM622 electrodes

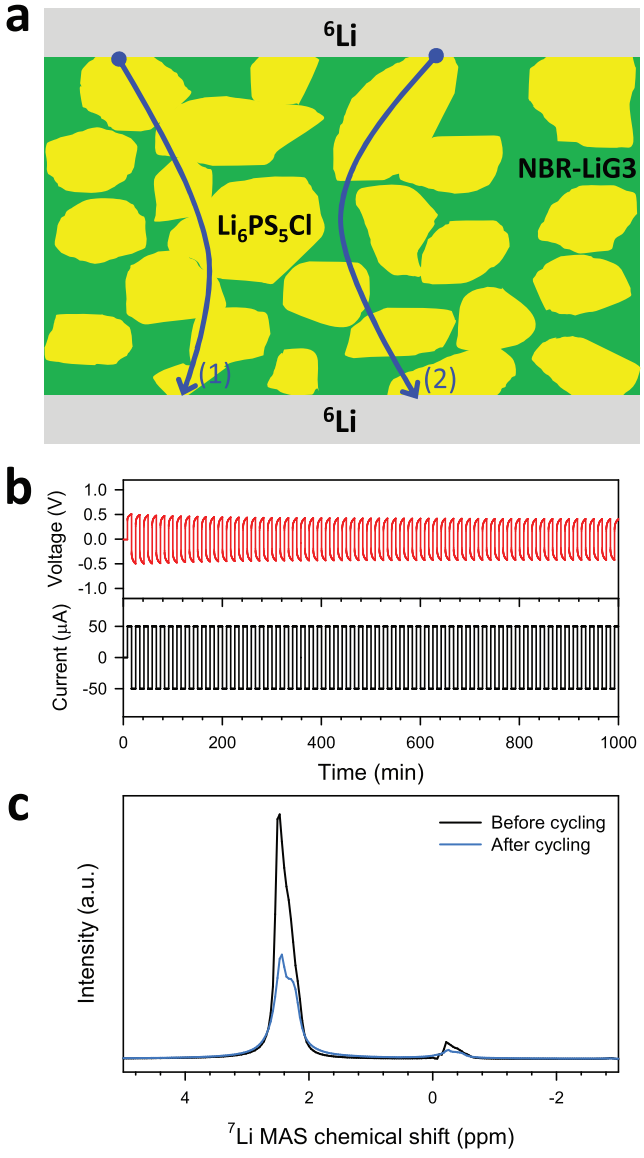

Figure 3. MAS ^{7}Li NMR results using $^6Li^+$-ion nonblocking symmetric cells (^{6}Li/LPSCl–NBR–LiG3/^{6}Li). a) Schematic diagram of the ^{6}Li/LPSCl–NBR–LiG3/^{6}Li cells. Li^+ conduction pathways in the composite SEs are shown (1, 2). b) Voltage profile obtained by consecutive charging and discharging at a constant current of 50 μA. c) MAS ^{7}Li NMR spectra of LPSCl–NBR–LiG3 before and after cycling. The peaks at ≈2.5 and −0.25 ppm are attributed to Li from LPSCl and NBR–LiG3, respectively.

without and with LiG3 (1.0 and 3.5 wt%) at 0.1 C (0.26 mA cm^{-2}) are shown in Figure 4a. The NCM622 ASLB electrodes without LiG3 showed only 80.0% capacity (144 mA h g^{-1}) of the ones using conventional liquid electrolytes (179 mA h g^{-1}; Figure S6, Supporting Information). The use of Li^+-conductive NBR–LiG3 binder resulted in the decreased overpotential and correspondingly dramatic increase in discharge capacity: 158 and 174 mA h g^{-1} for 1.0 and 3.5 wt% LiG3, respectively. The latter corresponds with 97.2% capacity of the liquid-electrolyte cells, which is unprecedented for sheet-type ASLB electrodes.[5,16,28,29,34] Moreover, the first-cycle Coulombic efficiencies increased from 78% without LiG3 to 86% and 90% with 1.0 and 3.5 wt% LiG3, respectively. The trend in rate capability was also in line with the one in capacity (Figure 4b). The NCM622 electrodes with 3.5 wt% LiG3 exhibited a capacity of 116 mA h g^{-1} at 1 C, which is approximately twice for the one without LiG3 and comparable to that of the conventional dry-mixed electrode without using binders.[29] The NCM622 electrode with LiG3 showed the stable cycling stabilities as shown in the inset in Figure 4b. Moreover, the NCM622 electrodes using NBR–LiG3 exhibited the decent cycling behavior at elevated temperature of 60 °C (Figure S7, Supporting Information). It is worth to be noted that momentary formation of free glyme in the SILs, which may cause side reaction, is unavoidable owing to dynamic solvation/desolvation nature or during charge-transfer reaction.[42] The good stability of NCM622 electrodes with LiG3 may be explained by shorter lifetime of free glyme (≈10^{-4} s) than the time constants for any undesirable side reactions.[42]

The Nyquist plots of NCM622 electrodes in Figure 4c shows the depressed semicircles followed by the Warburg tails, which are attributed to the interfacial resistance and Li^+ diffusion in NCM622, respectively.[15,29,56] The amplitude of semicircle decreased from 14.8 to 10.4 Ω by using the NBR–LiG3 binder, indicating the improvement in interfacial ionic contacts.[15,57] Transient charge–discharge voltage profiles obtained by galvanostatic intermittent titration technique (GITT) for NCM622 electrodes without and with LiG3 and their corresponding polarization curves are plotted in Figure 4d. The lowered polarization for the electrodes with LiG3 than without LiG3 is observed in the whole range. Furthermore, surface coverage values of NCM622 by electrolytes were extracted by analyzing the transient voltage profiles (see Supporting Information for details).[15] The surface coverage value increased from 27% to 42% by using NBR–LiG3. Also, Li^+ conductivities of NCM622 electrodes, obtained using electron-blocking Li–In/LPSCl/electrodes/LPSCl/Li–In symmetric cells, showed the higher value with LiG3 (2.0×10^{-4} S cm^{-1}) than without LiG3 (1.2×10^{-4} S cm^{-1}) (Figure S8, Supporting Information), indicating the facilitated Li^+-ionic pathways paved through the polymeric binders. So far, all the complementary electrochemical analysis results of the capacity (Figure 4a), the rate capability (Figure 4b), electrochemical impedance spectroscopy (EIS) (Figure 4c), GITT (Figure 4d), and electron-blocking cells (Figure S8, Supporting Information) unequivocally verify the enhanced ionic contacts and pathways enabled by the Li^+-conductive NBR–LiG3 binders.

The degree of utilization of NCM622 was estimated by ex situ XRD measurements of the electrodes at different state-of-charge (Figure 4e). From the peak position of the (003) plane of NCM622, the amount of Li in NCM622 could be compared. As the NCM622 electrode was charged to 4.3 V (vs Li/Li^+), the (003) peak shifted from 18.6° to lower angle (≈18.3°). This is due to the expansion of lattice along the *c*-axis, which is explained by the increased electrostatic repulsion between the M–O slabs in the layered structure.[27,58] After discharge to 3.0 V (vs Li/Li^+), the (003) peaks were shifted back to higher angle. Importantly, the peak position after discharge for the NCM622 electrode without LiG3 appeared to be more negative than that for the one with LiG3, indicating that less Li^+ is

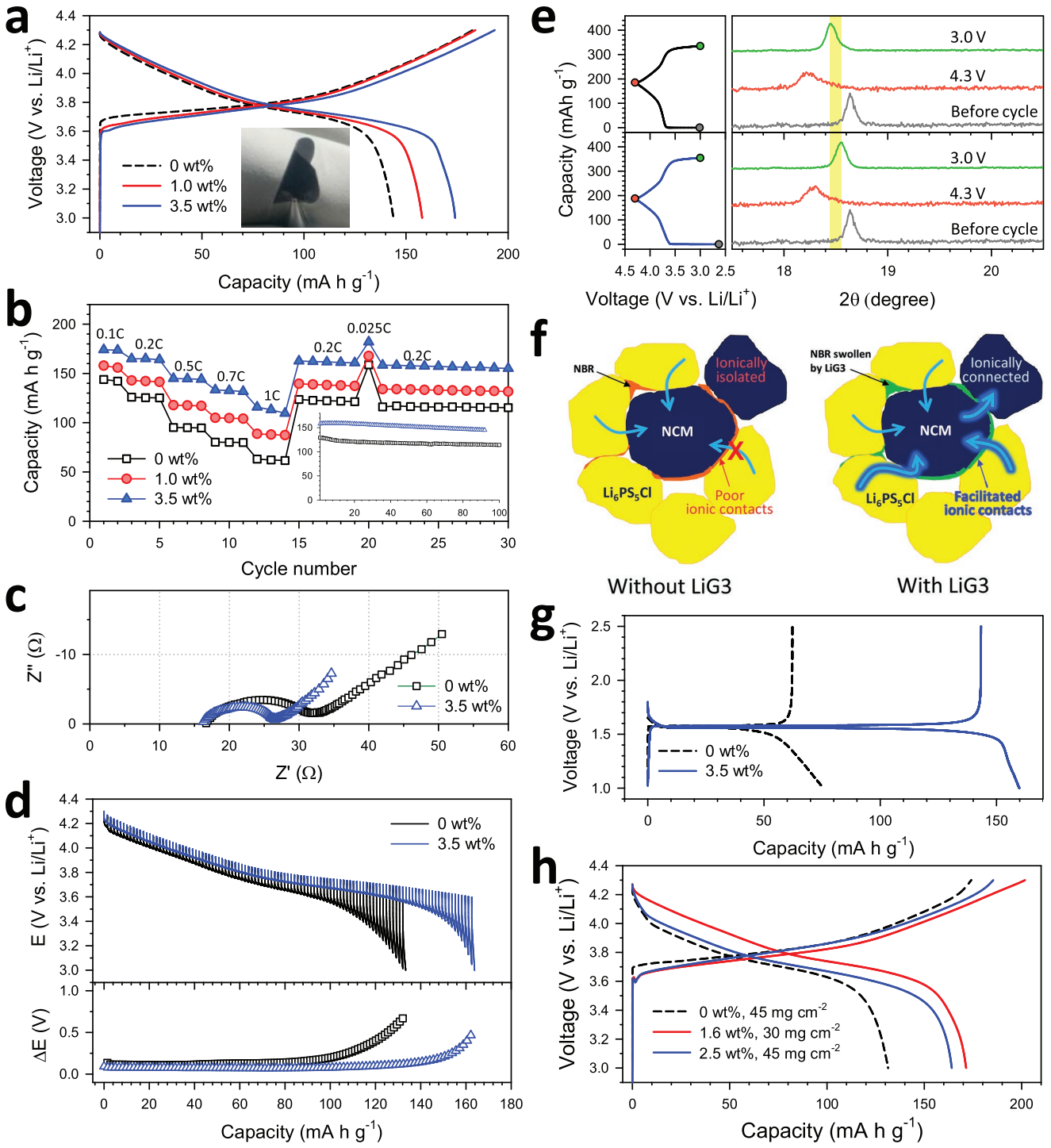

Figure 4. Comparative electrochemical characterizations of NCM/Li–In and LTO/Li–In all-solid-state cells at 30 °C, depending on the presence of LiG3 in the slurry-fabricated sheet-type electrodes. a) First-cycle charge–discharge voltage profiles at 0.1 C, b) rate capabilities, c) Nyquist plots, and d) transient voltage profiles and their corresponding polarization plots obtained by GITT for NCM622 electrodes without and with LiG3 (3.5 or 1.0 wt%). Photograph of the as-prepared electrodes with NBR–LiG3 is shown in the inset in (a). The cycling performances at 0.2 C are shown in the inset in (b). e) Ex situ XRD patterns showing (003) peaks for NCM622 at different states of charge for the electrodes. The corresponding charge–discharge voltage profiles at 0.1 C are shown in the left panel. f) Schematic diagram illustrating microstructures of NCM electrodes without and with LiG3. The blue arrows highlighted indicate Li^+ ionic pathways enabled by LiG3. g) First-cycle discharge–charge voltage profiles of LTO electrodes without and with LiG3 at 0.1 C. h) First-cycle charge–discharge voltage profiles for ultrathick (≈200 µm) NCM711 electrodes without and with LiG3 (1.6 or 2.5 wt%) at 0.025 C. Note that mass loadings for the data in (a–e) and (h) are 15 and 45 (or 30) mg cm^{-2}, respectively. Weight fraction for the data in (a–e) and (h) are 70.0 and 80.0 (or 83.0) wt%, respectively. The detailed specification of electrodes is provided in Table S4 in the Supporting Information.

intercalated back into NCM622 in the electrodes without LiG3 than with LiG3. This result evidences the incomplete utilization of active materials. This should be because of the slow kinetics associated with poor Li^+-ionic contacts and/or pathways that could be solved by employing the Li^+-conductive binders, consistent with the complementary electrochemical analysis results (Figure 4; Figure S8, Supporting Information). Also, a possible contribution by alleviated detrimental side reaction at interfaces by the Li^+-conductive binders is not ruled out.

The enhancement in electrochemical performance by the use of Li^+-conductive binder, NBR–LiG3, is more dramatic when sheet-type LTO electrodes were tested (Figure 4g; Table S4, Supporting Information). The LTO electrodes employing NBR–LiG3 with 3.5 wt% of LiG3 showed more than twice higher discharge capacity (160 mA h g^{-1}) of those using conventional Li^+-insulating NBR (76 mA h g^{-1}). The sheet-type NCM711 electrodes using NBR-LiG3 with ultrahigh mass loading (45 or 30 mg_{NCM711} cm^{-2}) and higher fraction of active material (80.0 or 83.0 wt% of NCM711) were also tested (Figure 4h). Cross-sectional FESEM images and the corresponding EDXS elemental maps show dense microstructure and homogeneous distribution of electrode components of NCM711, LPSCl, and NBR-LiG3 (Figure S9, Supporting Information). By the use of NBR–LiG3 (1.6 or 2.5 wt% LiG3), the first-cycle discharge capacity at 0.025 C was drastically increased from 131 (0 wt% LiG3) to 172 or 164 mA h g^{-1}.

Finally, different kinds of slurry-fabricable SIL-based Li^+-conductive binders could be derived. Although PMMA and PS are soluble into DBM (Table S2, Supporting Information), their glass transition temperature (T_g) is above 95 °C (Table S2, Supporting Information), indicating the brittleness at room temperature which is inappropriate to be used as the binder. However, they could be plasticized by addition of the SIL, LiG3, forming sheet-type electrodes with acceptable mechanical properties of flexibility and good adhesion.[59,60] While polyethylene oxide (PEO) itself is insoluble into xylene, PEO or PEO–LiG3 could become soluble in DBM. In consistent with the results for the NCM622 electrodes using NBR–LiG3, the electrodes using PMMA–LiG3, PS–LiG3, and PEO–LiG3 exhibited the increased capacities, compared with the ones without LiG3 (Figure S10, Supporting Information). Also, the sheet-type electrodes made of NBR with SILs using different kinds of solvent (G4: tetraethylene glycol dimethyl ether) or salt (LiBETI: lithium bis(trifluoromethanesulfonyl) imide) (Li(G4)TFSI and Li(G4)BETI) resulted in the similar capacities to those using LiG3 (Figure S11, Supporting Information). In short, these results highlight the generalized application of the slurry-fabricable SIL-based Li^+-conductive binders for ASLBs.

In the course of further investigation for optimal solvents in additional aspects such as toxicity and vapor pressure, butyl butyrate (BB) used in food additives has caught our attention. Despite the presence of ester group, it shows negligible reactivity with sulfide SEs, which may be rationalized by steric effects of the bulky alkyl groups. In addition, BB dissolves polybutadiene (PB) with SILs (Figure S12, Supporting Information), has low vapor pressure (1.81 mmHg at 25 °C), and is nontoxic (Table S5, Supporting Information). The NCM711 electrodes prepared from a slurry using BB and PB-Li(G4)BETI show remarkably increased capacity, compared with those without Li(G4)BETI (Figure S12, Supporting Information), which is consistent with the results of electrodes fabricated using DBM.

Ragone plot is shown for ASLBs employing slurry-fabricated sheet-type and dry-mixed electrodes for ASLBs in **Figure 5** (detailed characteristics are also shown in Table S6 in the Supporting Information). For the dry-mixed electrodes, both power and energy densities for $LiMO_2$ (M = Co, Ni, Mn) electrodes are superior to those for sulfide electrode materials such as S, Li_2S, and metal sulfides (Figure 5b). This is attributed to higher fraction of active materials in the electrodes and higher operating voltages for $LiMO_2$ than for sulfide electrode materials.[5] Slurry fabrication of sheet-type $LiMO_2$ electrodes leads to significantly lowered energy and power densities (Figure 5a), which must be due to the presence of insulating polymeric binders.[5,16,29] The sheet-type NCM electrodes employing NBR–LiG3 in this work exhibit drastically increased energy and power densities (maximum 73 W h kg^{-1} and 3.9 W kg^{-1} (based on the mass of electrodes and SE layer). Considering that the thickness of SE layer could be reduced less than 100 μm and Li–In electrodes could be replaced by graphite ones, the energy and power densities could be increased to 234 W h kg^{-1} and 20 W kg^{-1}, respectively. The energy density value of 234 W h kg^{-1} is higher than that for commercialized LIBs (100–200 W h kg^{-1}).[4,61] Furthermore, if Li metal (thickness of 100 μm) is enabled, a high energy density of 348 W h kg^{-1} could be obtained.

In summary, a new scalable hybridization protocol for SIL-based Li^+-conductive polymeric binders with sulfide SEs for practical ASLB electrodes were developed successfully. The slurry fabrication process was rationally designed considering the interactions among four components of the solvents such as DBM, SILs, sulfide SEs, and polymeric binders, in terms of the interplay between the miscibility of liquids and the intactness of liquids with sulfide SEs. The flexible sheet–type NCM and LTO electrodes using Li^+-conductive NBR–LiG3 binders for ASLBs were fabricated successfully via the scalable slurry process, demonstrating the significantly enhanced electrochemical performances (first-cycle discharge capacities of 174 mA h $g_{NCM622}{}^{-1}$ and 160 mA h $g_{LTO}{}^{-1}$), compared with those using the conventional NBR binder (144 mA h $g_{NCM622}{}^{-1}$ and 76 mA h $g_{LTO}{}^{-1}$). The NBR–LiG3 rendered the facilitated Li^+ ionic contacts and pathways in the resulting electrodes, which was confirmed unequivocally by the complementary analysis from the electrochemical and ^7Li NMR measurements. Moreover, the promising performance of NCM711 electrodes using NBR–LiG3 with ultrahigh mass loading (45 mg cm^{-2}) and high weight fraction of active material (≥80 wt%) was demonstrated (7.4 mA h cm^{-2}). Finally, the Li^+-conductive binders made of different kinds of polymeric binders (PMMA, PEO, and PS) and SILs (Li(G4)TFSI and Li(G4)BETI) highlighted the expandability of the as-developed technology. Also, this unique slurry fabrication protocol worked for an alternative slurry-solvent BB with nontoxicity and appropriate vapor pressure. We believe that our results will ignite interests in development of hybrid materials and open a new avenue in practical ASLB technologies.

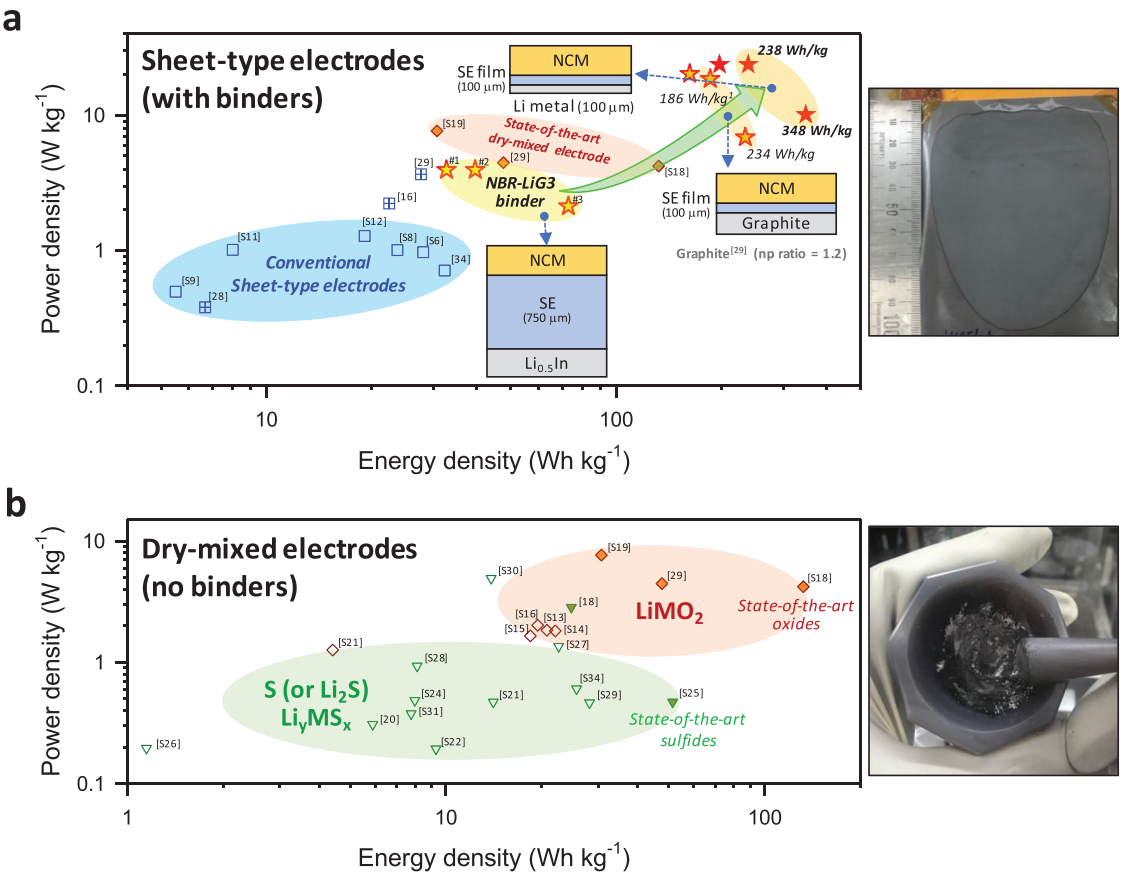

Figure 5. Ragone plots for ASLBs employing a) slurry-fabricated sheet-type and b) dry-mixed electrodes. Note that both energy and power densities for sheet-type electrodes employing NBR–LiG3 in this work are far superior to those for the conventional sheet–type electrodes. For fair comparison, the energy and power densities were calculated based on the use of 150 mg of SE layer and 100 mg of $Li_{0.5}In$ for a cell with a diameter of 13 mm. Photographs of a sheet-type electrode made of NBR–LiG3 and a dry mixture of active materials, SEs, super C65 are also shown in the right of (a) and (b), respectively.

Experimental Section

Preparation of Materials: Li_6PS_5Cl was prepared by ball-milling (Pulverisette 7 PL, Fritsch GmbH) and subsequent heat treatment under Ar atmosphere. A stoichiometric mixture of Li_2S (99.9%, Alfa-Aesar), P_2S_5 (99%, Sigma Aldrich), and LiCl (99.99%, Sigma Aldrich) was ball-milled at 600 rpm for 10 h in a ZrO_2 vial with ZrO_2 balls. The resulting powders were annealed at 550 °C for 5 h. $LiNi_{0.6}Co_{0.2}Mn_{0.2}O_2$ and $LiNi_{0.7}Co_{0.15}Mn_{0.15}O_2$ were coated by $LiNbO_3$ (1.4 wt%) via a wet-chemical method using lithium ethoxide (95%, Sigma Aldrich) and niobium ethoxide (99.95%, Sigma Aldrich).[16] The SILs were prepared by blending an equimolar anhydrous glymes (G3 (99%, Sigma Aldrich) or G4 (≥99%, Sigma Aldrich)) and Li salts (LiTFSI (lithium bis(trifluoromethane)sulfonimide, 99.95%, Sigma Aldrich) or LiBETI (lithium bis(pentafluoroethanesulfonyl)imide, 98%, TCI Corp.)). LPSCl–NBR–LiG3 composites were fabricated from a wet-slurry using DBM (99%, Sigma Aldrich) as the solvent and NBR (Sigma Aldrich) as the binder. All the liquids (G3, G4, DBM, and BB) and solids (LiTFSI, LiBETI, and NBR) used for the slurries were dried using molecular sieves (4 Å, DAEJUNG) and at 100 °C under vacuum, respectively.

Fabrication of Electrodes: The wet-slurries consisting of targeted weight ratios of active materials, binders, super C65, and SILs in slurry-processing solvents (DBM or BB) were coated on current collectors (Al or Ni) by doctor-blade method, followed by drying under vacuum at 60 °C (or 120 °C). All the processes for fabricating electrodes were conducted in an Ar-filled dry glove box. The electrode compositions are listed in Table S4 in the Supporting Information.

Material Characterization: For the XRD measurement, the samples sealed by Be window were mounted on a D8-Bruker Advance diffractometer (Cu K_α radiation: 1.54056 Å) at 40 mA and 40 kV. The static and MAS ^{7}Li NMR spectra were recorded using a Varian VNMRS 600 with 1.6 mm MAS HXY triple-resonance probe at Larmor frequencies of 233 MHz. The spinning rate for MAS ^{7}Li NMR measurements was 25 kHz. The chemical shift was referenced to LiCl at 0 ppm at 25 kHz of a spinning rate. The FESEM images and the EDXS elemental maps were obtained using a JSM-7000F (JEOL).

Electrochemical Characterization: The Li–In (nominal composition: $Li_{0.5}In$) as the counter and reference electrodes were prepared by ball-milling In (Aldrich, 99%) and Li (FMC Lithium Corp.) powders according to the previous report.[16] The SE layers were formed by pelletizing 150 mg of LPSCl powders under 370 MPa. Then, the NCM electrodes and the Li–In electrodes were put on each side of the SE layers. Finally, all-solid-state NCM/Li–In cells were obtained by pelletizing at 370 MPa at room temperature. Galvanostatic charge–discharge cycling test was carried out at 30 °C between 3.0 and 4.3 V (vs Li/Li^+). The EIS data were collected with an amplitude of 10 mV and frequency range from 10 mHz to 1 MHz using an Iviumstat (IVIUM Technologies Corp.). For the EIS measurements, the cells were charged to 4.3 V (vs Li/Li^+) at 0.1 C at first cycle, followed by rest for 3 h. The GITT measurements were carried out with a pulse current of 1.3 mA cm^{-2} (0.5 C) for 60 s and rest for 2 h. For tracking Li^+ pathways, $^6Li^+$-ion nonblocking symmetric cells of ^6Li/LPSCl–NBR–LiG3/^6Li were assembled as follows. ^6Li foils were attached to both sides of the LPSCl–NBR–LiG3 pellets. The ^6Li foils were prepared by compressing ^6Li chunk (95%, Sigma Aldrich).

All the procedures to fabricate all-solid-state cells were performed in a polyaryletheretherketone (PEEK) mold (1.33 cm^2) with two Ti metal rods. The all-solid-state cells were tested under ≈70 MPa.

Supporting Information

Supporting Information is available from the Wiley Online Library or from the author.

Acknowledgements

This research was supported by Hyundai Motors, by the Technology Development Program to Solve Climate Changes and by Basic Science Research Program of the National Research Foundation (NRF) funded by the Ministry of Science & ICT (grant no. NRF-2017M1A2A2044501 and 2018R1A2B6004996), and by the Materials and Components Technology Development Program of MOTIE/KEIT (grant no. 10077709).

Conflict of Interest

The authors declare no conflict of interest.

Keywords

binders, composite electrodes, solid electrolytes, solid-state batteries, super-concentrated electrolytes

Received: September 20, 2018
Revised: February 2, 2019
Published online: March 5, 2019

[1] J. B. Goodenough, Y. Kim, *Chem. Mater.* **2010**, *22*, 587.
[2] M. M. Thackeray, C. Wolverton, E. D. Isaacs, *Energy Environ. Sci.* **2012**, *5*, 7854.
[3] D. Larcher, J. M. Tarascon, *Nat. Chem.* **2015**, *7*, 19.
[4] R. Schmuch, R. Wagner, G. Hörpel, T. Placke, M. Winter, *Nat. Energy* **2018**, *3*, 267.
[5] K. H. Park, Q. Bai, D. H. Kim, D. Y. Oh, Y. Zhu, Y. Mo, Y. S. Jung, *Adv. Energy Mater.* **2018**, *8*, 1800035.
[6] J. Janek, W. G. Zeier, *Nat. Energy* **2016**, *1*, 16141.
[7] K. Kerman, A. Luntz, V. Viswanathan, Y.-M. Chiang, Z. Chen, *J. Electrochem. Soc.* **2017**, *164*, A1731.
[8] A. Manthiram, X. Yu, S. Wang, *Nat. Rev. Mater.* **2017**, *2*, 16103.
[9] E. Rangasamy, Z. Liu, M. Gobet, K. Pilar, G. Sahu, W. Zhou, H. Wu, S. Greenbaum, C. Liang, *J. Am. Chem. Soc.* **2015**, *137*, 1384.
[10] A. Sharafi, E. Kazyak, A. L. Davis, S. Yu, T. Thompson, D. J. Siegel, N. P. Dasgupta, J. Sakamoto, *Chem. Mater.* **2017**, *29*, 7961.
[11] X. Han, Y. Gong, K. K. Fu, X. He, G. T. Hitz, J. Dai, A. Pearse, B. Liu, H. Wang, G. Rubloff, Y. Mo, V. Thangadurai, E. D. Wachsman, L. Hu, *Nat. Mater.* **2017**, *16*, 572.
[12] Y. Yan, R.-S. Kühnel, A. Remhof, L. Duchêne, E. C. Reyes, D. Rentsch, Z. Łodziana, C. Battaglia, *Adv. Energy Mater.* **2017**, *7*, 1700294.
[13] Y. Kato, S. Hori, T. Saito, K. Suzuki, M. Hirayama, A. Mitsui, M. Yonemura, H. Iba, R. Kanno, *Nat. Energy* **2016**, *1*, 16030.
[14] Y. Wang, W. D. Richards, S. P. Ong, L. J. Miara, J. C. Kim, Y. Mo, G. Ceder, *Nat. Mater.* **2015**, *14*, 1026.
[15] K. H. Park, D. Y. Oh, Y. E. Choi, Y. J. Nam, L. Han, J.-Y. Kim, H. Xin, F. Lin, S. M. Oh, Y. S. Jung, *Adv. Mater.* **2016**, *28*, 1874.
[16] D. H. Kim, D. Y. Oh, K. H. Park, Y. E. Choi, Y. J. Nam, H. A. Lee, S.-M. Lee, Y. S. Jung, *Nano Lett.* **2017**, *17*, 3013.
[17] J. H. Woo, J. E. Trevey, A. S. Cavanagh, Y. S. Choi, S. C. Kim, S. M. George, K. H. Oh, S. H. Lee, *J. Electrochem. Soc.* **2012**, *159*, A1120.
[18] M. Chen, S. Adams, *J. Solid State Electrochem.* **2015**, *19*, 697.
[19] I.-H. Chu, N. Han, S. Hy, Y.-C. Lin, Z. Wang, Z. Xu, Z. Deng, Y. S. Meng, S. P. Ong, *ACS Appl. Mater. Interfaces* **2016**, *8*, 7843.
[20] X. Yao, N. Huang, F. Han, Q. Zhang, H. Wan, J. P. Mwizerwa, C. Wang, X. Xu, *Adv. Energy Mater.* **2017**, *7*, 1602923.
[21] J. Yue, M. Yan, Y.-X. Yin, Y.-G. Guo, *Adv. Funct. Mater.* **2018**, *28*, 1707533.
[22] Y. Seino, T. Ota, K. Takada, A. Hayashi, M. Tatsumisago, *Energy Environ. Sci.* **2014**, *7*, 627.
[23] K. Xu, *Chem. Rev.* **2004**, *104*, 4303.
[24] A. Sakuda, A. Hayashi, M. Tatsumisago, *Sci. Rep.* **2013**, *3*, 2261.
[25] A. Banerjee, K. H. Park, J. W. Heo, Y. J. Nam, C. K. Moon, S. M. Oh, S.-T. Hong, Y. S. Jung, *Angew. Chem., Int. Ed.* **2016**, *55*, 9634.
[26] F. P. McGrogan, T. Swamy, S. R. Bishop, E. Eggleton, L. Porz, X. Chen, Y.-M. Chiang, K. J. V. Vliet, *Adv. Energy Mater.* **2017**, *7*, 1602011.
[27] R. Koerver, W. Zhang, L. de Biasi, S. Schweidler, A. O. Kondrakov, S. Kolling, T. Brezesinski, P. Hartmann, W. G. Zeier, J. Janek, *Energy Environ. Sci.* **2018**, *11*, 2142.
[28] D. Y. Oh, D. H. Kim, S. H. Jung, J.-G. Han, N.-S. Choi, Y. S. Jung, *J. Mater. Chem. A* **2017**, *5*, 20771.
[29] Y. J. Nam, D. Y. Oh, S. H. Jung, Y. S. Jung, *J. Power Sources* **2018**, *375*, 93.
[30] J. Schnell, T. Guenther, T. Knoche, C. Vieider, L. Koehler, A. Just, M. Keller, S. Passerini, G. Reinhart, *J. Power Sources* **2018**, *382*, 160.
[31] Y. J. Nam, K. H. Park, D. Y. Oh, W. H. An, Y. S. Jung, *J. Mater. Chem. A* **2018**, *6*, 14867.
[32] W. Philip, *J. Polym. Sci., Part C: Polym. Symp.* **1966**, *12*, 169.
[33] S. Choi, T.-w. Kwon, A. Coskun, J. W. Choi, *Science* **2017**, *357*, 279.
[34] S. Ito, S. Fujiki, T. Yamada, Y. Aihara, Y. Park, T. Y. Kim, S.-W. Baek, J.-M. Lee, S. Doo, N. Machida, *J. Power Sources* **2014**, *248*, 943.
[35] H.-K. Tian, Y. Qi, *J. Electrochem. Soc.* **2017**, *164*, E3512.
[36] I. Osada, H. de Vries, B. Scrosati, S. Passerini, *Angew. Chem., Int. Ed.* **2016**, *55*, 500.
[37] X. L. Cheng, J. Pan, Y. Zhao, M. Liao, H. S. Peng, *Adv. Energy Mater.* **2018**, *8*, 1702184.
[38] Y. Yamada, A. Yamada, *J. Electrochem. Soc.* **2015**, *162*, A2406.
[39] Y. Yamada, K. Furukawa, K. Sodeyama, K. Kikuchi, M. Yaegashi, Y. Tateyama, A. Yamada, *J. Am. Chem. Soc.* **2014**, *136*, 5039.
[40] M. Cuisinier, P. E. Cabelguen, B. D. Adams, A. Garsuch, M. Balasubramanian, L. F. Nazar, *Energy Environ. Sci.* **2014**, *7*, 2697.
[41] L. Suo, O. Borodin, T. Gao, M. Olguin, J. Ho, X. Fan, C. Luo, C. Wang, K. Xu, *Science* **2015**, *350*, 938.
[42] K. Yoshida, M. Nakamura, Y. Kazue, N. Tachikawa, S. Tsuzuki, S. Seki, K. Dokko, M. Watanabe, *J. Am. Chem. Soc.* **2011**, *133*, 13121.
[43] K. Ueno, J. Murai, K. Ikeda, S. Tsuzuki, M. Tsuchiya, R. Tatara, T. Mandai, Y. Umebayashi, K. Dokko, M. Watanabe, *J. Phys. Chem. C* **2016**, *120*, 15792.
[44] D. Y. Oh, Y. J. Nam, K. H. Park, S. H. Jung, S.-J. Cho, Y. K. Kim, Y.-G. Lee, S.-Y. Lee, Y. S. Jung, *Adv. Energy Mater.* **2015**, *5*, 1500865.
[45] J. E. Huheey, E. A. Keiter, R. L. Keiter*Inorganic Chemistry: Principles of Structure and Reactivity*, 4th ed., HarperCollins College Publishers, New York **1993**.
[46] J. Gao, M. A. Lowe, Y. Kiya, H. D. Abruna, *J. Phys. Chem. C* **2011**, *115*, 25132.
[47] M. Tang, V. Sarou-Kanian, P. Melin, J.-B. Leriche, M. Ménétrier, J.-M. Tarascon, M. Deschamps, E. Salager, *Nat. Commun.* **2016**, *7*, 13284.
[48] X. Wang, H. Zhu, G. A. Girard, R. Yunis, D. R. MacFarlane, D. Mecerreyes, A. J. Bhattacharyya, P. C. Howlett, M. Forsyth, *J. Mater. Chem. A* **2017**, *5*, 23844.

[49] J. Zheng, M. Tang, Y.-Y. Hu, *Angew. Chem., Int. Ed.* **2016**, *55*, 12538.
[50] J. Zheng, Y. Y. Hu, *ACS Appl. Mater. Interfaces* **2018**, *10*, 4113.
[51] C. Wan, S. Xu, M. Y. Hu, R. Cao, J. Qian, Z. Qin, J. Liu, K. T. Mueller, J.-G. Zhang, J. Z. Hu, *ACS Appl. Mater. Interfaces* **2017**, *9*, 14741.
[52] S. Wenzel, S. J. Sedlmaier, C. Dietrich, W. G. Zeier, J. Janek, *Solid State Ionics* **2018**, *318*, 102.
[53] D. Wohlmuth, V. Epp, M. Wilkening, *ChemPhysChem* **2015**, *16*, 2582.
[54] F. Han, J. Yue, X. Zhu, C. Wang, *Adv. Energy Mater.* **2018**, *8*, 1703644.
[55] D. Zhang, B. Haran, A. Durairajan, R. E. White, Y. Podrazhansky, B. N. Popov, *J. Power Sources* **2000**, *91*, 122.
[56] S. H. Jung, K. Oh, Y. J. Nam, D. Y. Oh, P. Bruener, K. Kang, Y. S. Jung, *Chem. Mater.* **2018**, *30*, 8190.
[57] Y. E. Choi, K. H. Park, D. H. Kim, D. Y. Oh, H. R. Kwak, Y.-G. Lee, Y. S. Jung, *ChemSusChem* **2017**, *10*, 2605.
[58] Q. Wang, C.-H. Shen, S.-Y. Shen, Y.-F. Xu, C.-G. Shi, L. Huang, J.-T. Li, S.-G. Sun, *ACS Appl. Mater. Interfaces* **2017**, *9*, 24731.
[59] Y. Kitazawa, K. Iwata, S. Imaizumi, H. Ahn, S. Y. Kim, K. Ueno, M. J. Park, M. Watanabe, *Macromolecules* **2014**, *47*, 6009.
[60] Y. Kitazawa, K. Iwata, R. Kido, S. Imaizumi, S. Tsuzuki, W. Shinoda, K. Ueno, T. Mandai, H. Kokubo, K. Dokko, M. Watanabe, *Chem. Mater.* **2018**, *30*, 252.
[61] J. H. Lee, C. S. Yoon, J. Y. Hwang, S. J. Kim, F. Maglia, P. Lamp, S. T. Myung, Y. K. Sun, *Energy Environ. Sci.* **2016**, *9*, 2152.